Di Francesco, M., Giddings, P. F., Scott, M., Goodman, E., Dell'Anno, G., & Potter, K. (2016). Influence of laser power density on the mesostructure of thermoplastic composite preforms manufactured by Automated Fibre Placement. In International SAMPE Technical Conference. (Vol. 2016-January). Soc. for the Advancement of Material and Process Engineering.

Peer reviewed version

INFLUENCE OF LASER POWER DENSITY ON THE MESO-STRUCTURE OF THERMOPLASTIC COMPOSITE PREFORMS MANUFACTURED BY AUTOMATED FIBRE PLACEMENT

Mattia Di Francesco, Peter F. Giddings, Matt Scott, Ed Goodman, Giuseppe Dell'Anno
The National Composites Centre
Feynman Way Central, Bristol & Bath Science Park
Bristol UK BS16 7FS
Kevin Potter
Department of Aerospace Engineering, University of Bristol
Queen's Building, University Walk
Bristol UK BS8 1TR

ABSTRACT

Automated Fibre Placement is an established composite manufacturing technology for the deposition of carbon fibre reinforced thermoset materials. In recent years, implementation of suitably controlled laser heaters has enabled processing of high-performance thermoplastic matrix prepreg at a rate compatible with industrial environments. Laser-assisted Automated Fibre Placement is often characterised solely in terms of the supplied laser power or the measured temperature at the convergence between the layup roller and the substrate, referred to as the "nip-point". However, the thermally affected zone extends beyond the nip-point, and the thermal profile in its vicinity determines the meso-structure of the deposited thermoplastic composite laminate. Specifically, the void fraction and degree of inter-ply bonding.

An infrared thermal camera and embedded thermocouples were used to determine the thermal profile resulting from the use of two laser lenses, delivering different laser beam cross-sectional depths. The resulting laminate structure and void content were assessed by optical microscopy of polished cross-sections and ultrasonic testing.

This work demonstrates that, for constant nip point temperature, the size of the laser heated zone relative to the nip-point alters the resulting void fraction and inter-ply bonding.

1 INTRODUCTION

Laser-assisted Automated Fibre Placement (AFP) has been proposed as a possible manufacturing technology for the deposition of high performance, semi-crystalline carbon fibre reinforced thermoplastic materials [1], either as a single step *in-situ* consolidation process delivering a finished laminate [2], or as the material deposition step (preforming) in a multi-step process involving post-processing in an autoclave, press or oven [3]. The post-process (if any), and the finished laminate quality criteria determine the requirements for the laminate/preform produced by the AFP machine [4].

The laser-assisted AFP process can be characterised in terms of the machine parameters (laser power, deposition speed, compaction force, etc.) or in terms of the temperature at the convergence between the layup roller and the substrate, namely the nip point, measured by non-contact means. The processing parameters (time dependent temperature and pressure) are not always reported in the literature as their characterisation requires relatively complex experimental setups and/or numerical simulation of the process. However, Maurer and Mitschang [5] showed through process simulation of the laser-assisted AFP process that increasing the laser beam height widens the process window. Similarly, Stokes-Griffin and Compston [6] suggested that increasing the heated length at high deposition speed (400 mm/s) would result in a broader process window. This makes it questionable whether the machine parameters and/or the nip-point temperature alone are sufficient to characterise the process and suggests that further investigation into the effect of the laser beam cross-section is required.

This paper addresses this issue by determining, through experiments and numerical simulation, the thermal profile resulting from the use of two laser homogeniser optics, delivering different laser beam cross sectional depths and by analysing the resulting preform meso-structure.

2 EXPERIMENTAL SETUP AND SIMULATION METHOD

2.1 Machine details

A state-of-the-art industrial Automated Fibre Placement machine by Coriolis Composites was used for this work (Figure 1). The machine is capable of simultaneously depositing up to eight 6.35 mm wide continuous tapes at a nominal maximum speed of 1000 mm/s. The heat source for the process is a Laserline GmbH LDF 6000-100 6 kW fibre-coupled diode laser (two diode stacks at $\lambda = 975 \pm 10$ nm and two at $\lambda = 1025 \pm 10$ nm). The laser is installed remotely from the fibre placement head and the beam is guided through a fibre optic cable to a homogeniser optic to deliver a nominally homogeneous (≈ 7 % power variation across the course width) and rectangular laser beam. Two laser optics are available at the National Composites Centre, both delivering a 57 mm wide beam at the focal point, but having different laser spot heights: 8 mm and 28 mm. The laser lens mounting enables the beam to be targeted to the desired location by rotating it around a pivot point before being fixed in place for the lay-up. Similarly, the optical unit can be moved back and forth within its structure to account for the different focal distance between different optics. Other machine configuration parameters which can be adjusted and which affect the temperature distribution in the process, but were kept constant for the purpose of this work are: the head tilt ($\Theta = -7°$), the roller design (70 mm diameter) and material (40 Shore hardness silicone), the compaction force (1025 ±3 N at 95 % confidence interval) and the air pressure of the forced convection roller cooling system (6 bar).

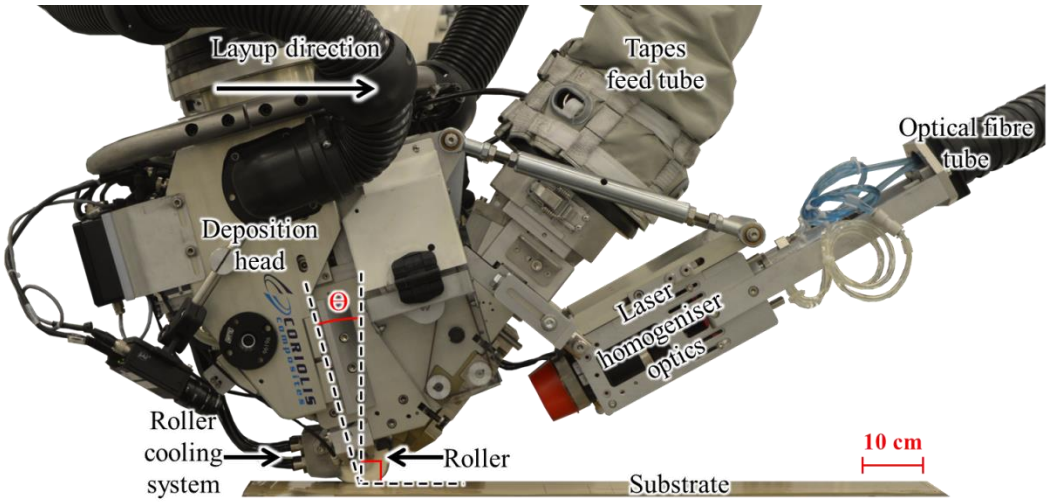

Figure 1: Laser-assisted Coriolis Composites Automated Fibre Placement (AFP) machine head showing the installation of the laser homogeniser optics.

2.2 Dimensions and setup design

The laser optic was setup according to the parameters in Table 1, as illustrated in Figure 2.

Table 1: Laser power distribution and laser beam angle for the 57x8 and the 57x28 mm laser spot cases.

Setup I.D.	Laser beam width, mm	Laser beam height, mm	Power split substrate (a) / tapes (b)	Substrate heated length (a_1), mm	Tapes heated length (b_1), mm	Angle (α), degree
57 x 28 mm	57	28	85 % / 15 %	69.0	20.2	20
57 x 8 mm (nip point)	57	8	70 % / 30 %	18.0	21.2	18
57 x 8 mm (substrate)	57	8	100 % / 0 %	24.6	0.0	19

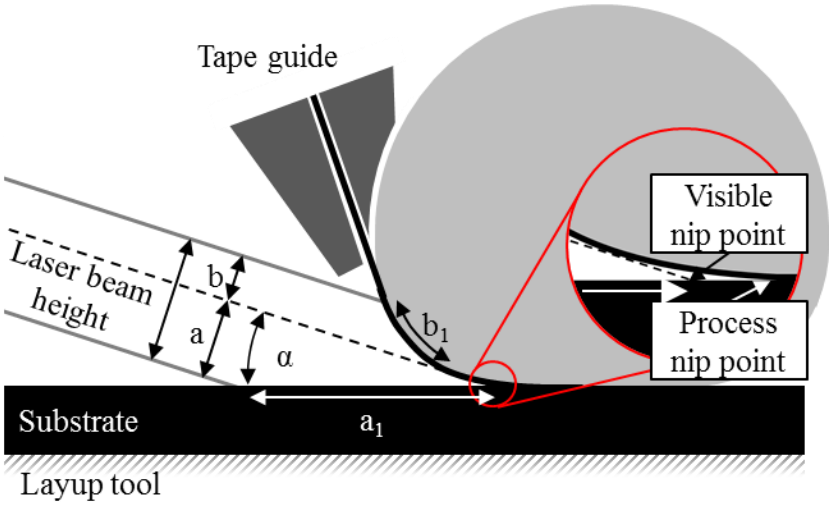

Figure 2: Laser beam target, power split and temperature measurement location.

A flat, unidirectional, 16 ply thick, 650 mm long test strip made up of 8 tapes and deposited in a single 50.8 mm wide course, was laid up at a constant speed (i.e. no acceleration and deceleration were programmed in the robot movements) of 400 mm/s for each of the three manufacturing setups outlined in Table 1. The strips were laid up over a 150 μm thick Poly Ether Ether Ketone (PEEK) film (Victrex® APTIV® 1000) vacuumed to the surface of an aluminium tool. The laser power was set to 4500 W and 3000 W respectively for the 57 x 28 mm and the 57 x 8 mm (nip point and substrate) setups.

Similarly, two, 8 ply thick, quasi-isotropic, 1100 x 400 mm panels were laid up. One with the 57 x 28 mm laser beam and one with the 57 x 8 mm laser beam targeting the substrate. The panels feature a 16 ply thick pad-up (total) on one side and an extra 50 mm wide frame around their contour. This consists of the first two plies and is used to prevent damage of the PEEK film over which the panel is laminated. The first two plies were programmed to layup at a constant deposition speed of 400 mm/s. The remaining 6 plies of the constant thickness section of the panel were programmed to feed and cut at 400 mm/s and layup at 800 mm/s. The 8 pad-up plies were programmed to feed and cut at a speed of 200 mm/s for increased accuracy, and layup at 800 mm/s. The programmed acceleration/deceleration was 1000 mm/s^2 and the machine reached the programmed maximum lay up speed of 800 mm/s only during the deposition of the 0 ° plies (along the long side of the panel), as expected.

The laser power was set to 4500 W and 3000 W respectively for the 57 x 28 mm and 57 x 8 mm (substrate) laser beam cross section case when laying up at a constant deposition speed of 400 mm/s and was set to vary linearly with the deposition speed to achieve a nominal constant nip point temperature of 360 °C. The preforms were not post-processed and this should be regarded as a part of further work.

The material was APC-2/AS4 145/34, a standard industrial carbon fibre PEEK prepreg supplied by Cytec Industries Inc and slit into 6.35 mm wide tapes. The characteristics of the as-supplied material were determined experimentally (Table 2).

Table 2: Characteristics of the as-supplied Cytec APC-2/AS4 145/34.

Property	**Value** (95% confidence interval)	**Characterisation method**
Surface roughness (arithmetic mean deviation of the roughness profile, R_a)	4.10 ±0.34 μm	Optical 3D microscopy at a magnification of 20x (≈ 1 μm/pixel) (ISO 4287 and ISO 13565)
Thickness	151.8 ± 24.2 μm	Optical microscopy of polished cross sections at a magnification of 50x (0.20 μm/pixel)
Fibre volume fraction	56.7 ± 14.6 %	
Void content	1.3 ± 1.8 %	
Glass transition temperature	141.4 ± 2.8 °C (midpoint)	Differential Scanning Calorimetry (ASTM D3418)
Melting temperature	328.1 ± 2.3 °C (onset) 344.9 ± 1.9 °C (peak)	

2.3 Temperature measurement

The material surface temperature in the nip point region was measured using a FLIR A325 Long Wave Infrared (LWIR) (λ = 7.5-13 μm) thermal camera. The camera's infrared detector has a resolution of 320 x 240 pixels (≈ 0.5 mm/pixel). All recordings were made at 30 Hz.

The apparent emissivity of the material when imaged at an angle of 20° in the relevant temperature range (350-450 °C) was determined in accordance with the ASTM E1933 standard by comparing the temperature measured by the thermal camera with that measured by a thermocouple placed to be in intimate contact with the material surface. The apparent emissivity is 0.80. Other relevant parameters which affect the thermal camera temperature reading are the distance from the target (0.3 m) and the environmental conditions: ambient temperature (20 °C) and relative humidity (40 %).

The thermal camera was used to measure the substrate's surface temperature up to the visible nip point (Figure 2). The temperature in the bulk of the material was measured using a 25 μm diameter K-type thermocouple placed at the interface between the 9th and 10th ply in the middle of each strip. The thermocouples output was logged at 90 Hz. The data collected by the thermal camera together with those collected by thermocouples allowed characterising the full thermal history of one location of the laminate.

2.4 Numerical thermal simulation

In this work, in-process thermal history between the deposited material and the substrate was predicted using a numerical simulation tool for constant speed laser-assisted AFP processes developed at the National Composites Centre. The developed tool takes readily measured machine set-up and process control parameters and published material properties presented in [7] as inputs to solve a system of finite difference equations describing heat transfer within the laser-assisted AFP process.

To increase predictive accuracy, this work couples temperature-dependent variation of conductivity, specific heat capacity and density with predicted material temperature to capture the influence on thermal history of variance in thermal diffusivity within the process zone. Standard finite difference equations [7] for 2D thermal diffusion with anisotropic conductivity for tape and substrate volumes were implemented in MatLab R2013. Laser heat input was simulated as a uniformly distributed surface irradiation, with radiant power density incident on the substrate ($\dot{Q}_L$) described by Equation 1, where $\dot{Q}_L^0$ is the total delivered laser power and parameters a, a_1 and b are calculated geometrically as shown in Figure 2.

$$\dot{Q}_L = \frac{\dot{Q}_L^0 \times a}{w \times a_1 \times (a+b)} \quad (1)$$

The movement of the irradiated area during deposition was described using position-dependent boundary conditions on nodes at the heated surface. The surface boundary conditions (Figure 3) were modified at specified distances in front and behind the process nip point (Figure 2).

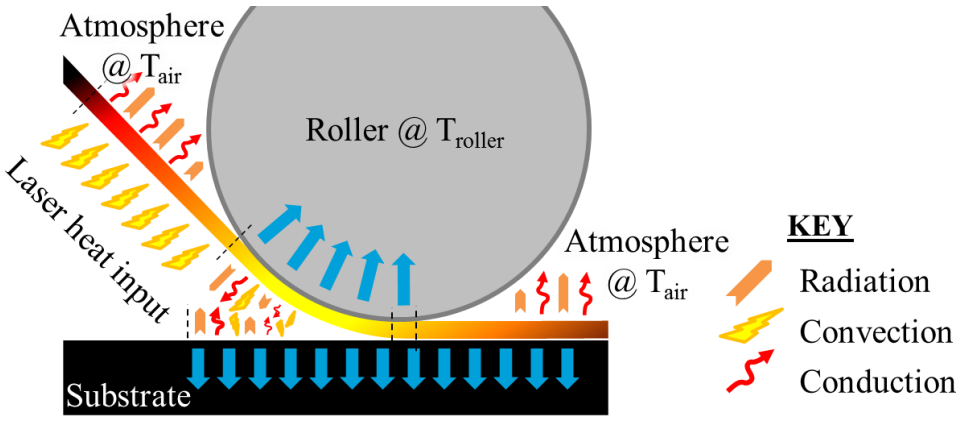

Figure 3: Schematic showing thermal diffusion mechanisms active in different regions of the process zone.

Boundary conditions describing natural convection and radiation between the process zone and the atmosphere were applied over the regions shown in Figure 3. Conduction at the interface between the process zone and the polymeric roller was not modelled. The PEEK interface ply between processed composite and the aluminium tool was discretely modelled as an isotropically conductive layer whose interface with the tool was described by a fixed temperature boundary condition set to the system initial temperature.

In the present work, the interfaces between the plies comprising the substrate were modelled as having a constant degree of intimate contact. The specified degree of contact was derived from post hoc physical measurement of the achieved degree of inter-ply contact for each experimental case. The influence of reduced inter-ply contact on through-thickness heat diffusion was modelled as a contact resistance proportional to degree of intimate contact as described in [8]. Contact at the interface between deposited tape and substrate was assumed to develop to its full value on first contact and remain unchanged during deposition of the subsequent plies.

The developed simulation was run for deposition of the tenth ply onto a substrate comprising nine constant thickness plies having uniform initial material and process conditions. Nodal values for temperatures and material properties describing heat transfer behaviour were stored to create a material-state history for the laminate throughout the laser-assisted AFP process. Spatially distributed material-state data were converted to a time-based process history for the constant velocity deposition for comparison with experimental data.

2.5 Sample inspection

Three samples were extracted from the central section of each unidirectional strip. These were potted, polished and imaged using an optical microscope at three locations across their width (Figure 4). A magnification of 20x was used (0.49 µm/pixel) and 10 images were tiled to produce each micrograph. The void content and the degree of intimate contact, the fraction of the total surface area in contact between two plies [9], were measured from the images using ImageJ (Figure 5).

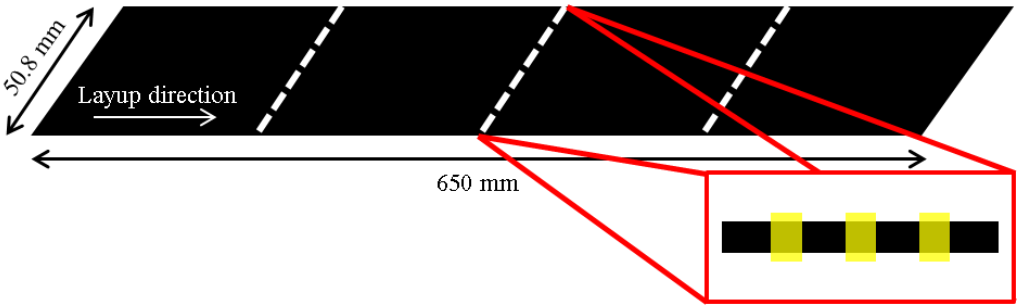

Figure 4: Sample extraction locations (white dashed lines) for microscopy (observed regions are in yellow).

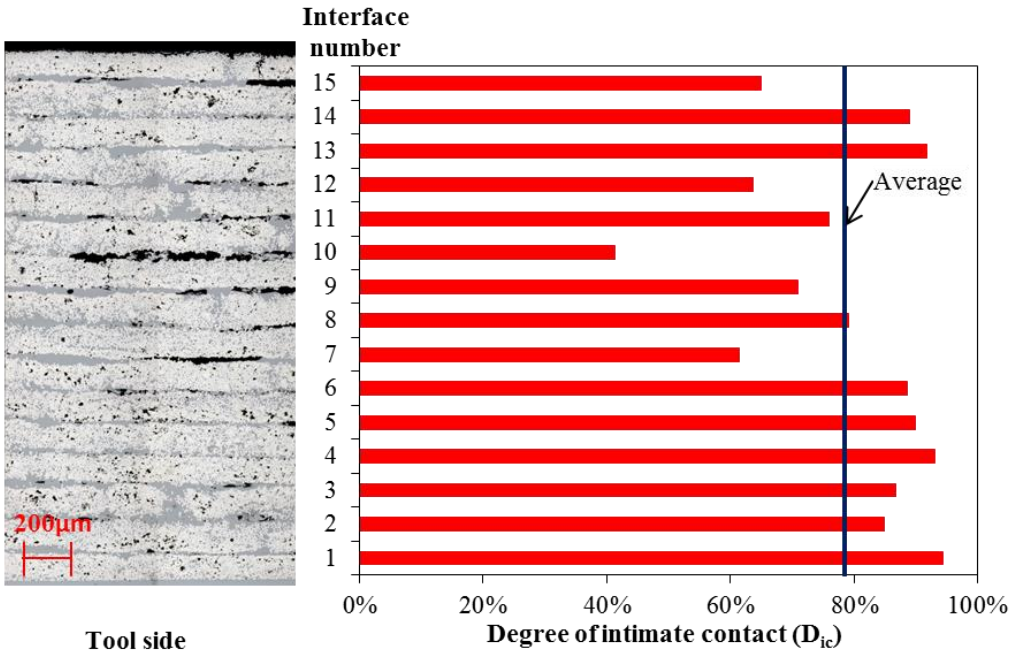

Figure 5: Thresholded micrographs of a polished cross section showing the inter- and intra-tape voids in black (left). Chart of the measured degree of intimate contact between the plies showing the average and the confidence interval (right). No D_{ic} through thickness gradient was observed ($p = 0.12 > 0.05$).

The panels were visually inspected during and after manufacture. Non-destructive through transmission ultrasonic scanning was performed on the preform at a scan pitch of 2 mm and a frequency of 5 MHz.

3 EXPERIMENTAL AND SIMULATION RESULTS

3.1 Experimentally determined and simulated thermal history

The temperature history, experimentally determined and simulated, of the interface between the 9^{th} and 10^{th} ply of the unidirectional strips during deposition of the 10^{th} to the 13^{th} ply is reported in Figure 6 to Figure 8, together with the pressure applied by the roller, the measured glass transition temperature (T_g) and the onset melt temperature (T_{om}) (Table 2). The temperature history was truncated below the T_g on cooling for the sake of clarity of the charts.

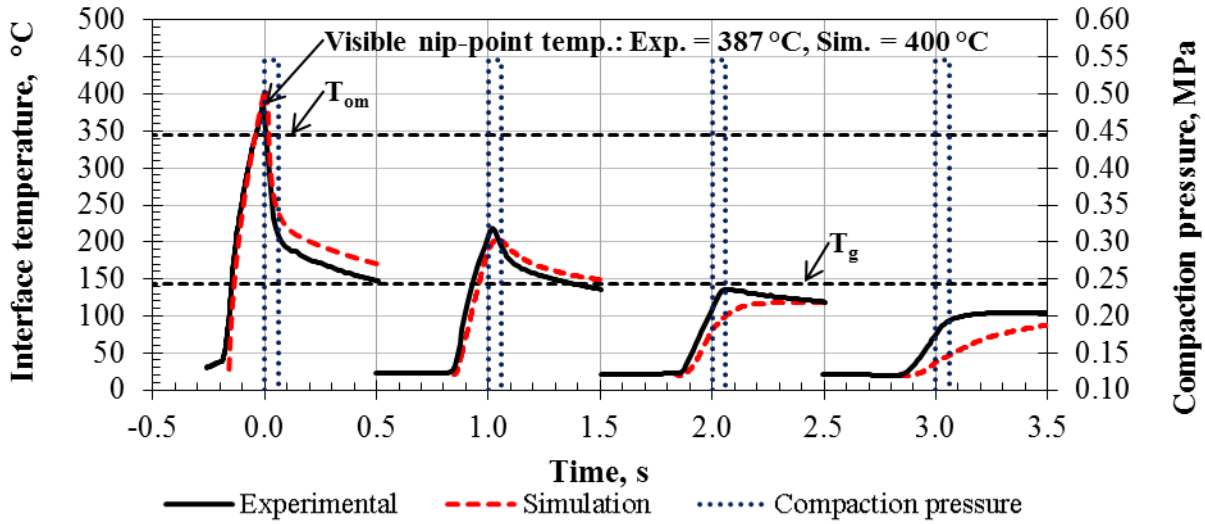

Figure 6: The temperature history of the interface between the 9th and 10th ply of the unidirectional strips during deposition of the 10th to the 13th ply, together with the approximated pressure applied by the roller, the measured glass transition temperature (T_g), the onset melt temperature (T_{om}) and the crystallisation temperature range (T_c) at a set laser power of 4500 W, a set deposition speed of 400 mm/s for 57 x 28 mm laser beam case.

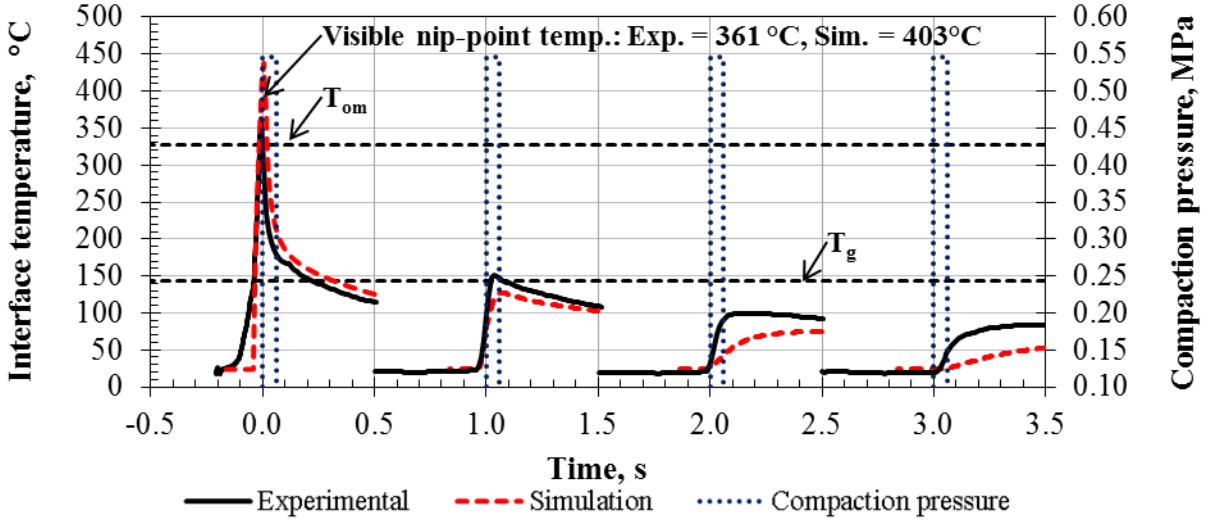

Figure 7: The temperature history of the interface between the 9th and 10th ply of the unidirectional strips during deposition of the 10th to the 13th ply, together with the approximated pressure applied by the roller, the measured glass transition temperature (T_g), the onset melt temperature (T_{om}) and the crystallisation temperature range (T_c) at a set laser power of 3000 W, a set deposition speed of 400 mm/s for 57 x 8 mm (nip point) laser beam.

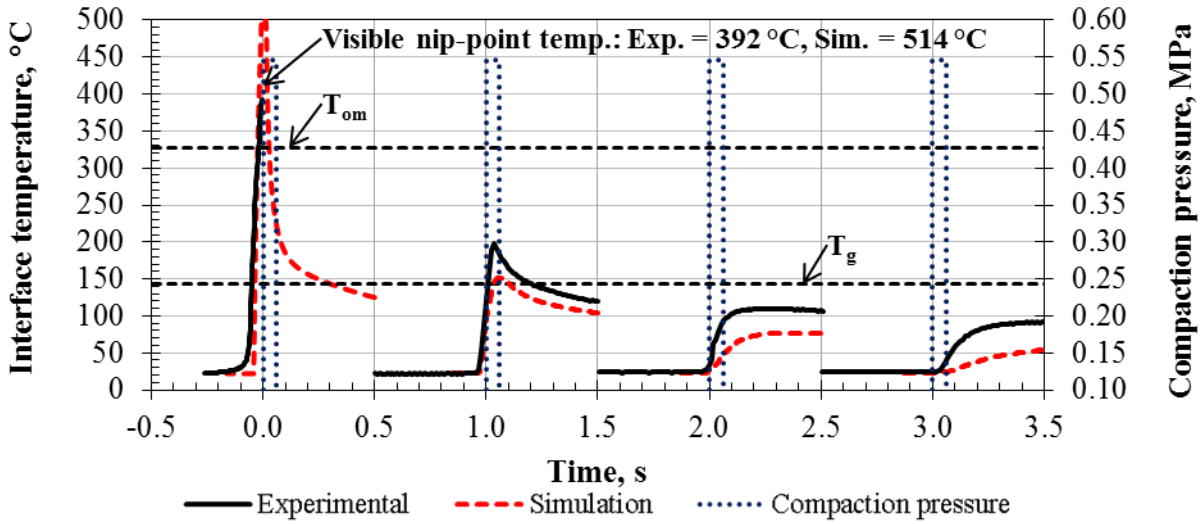

Figure 8: The temperature history of the interface between the 9th and 10th ply of the unidirectional strips during deposition of the 10th to the 13th ply, together with the approximated pressure applied by the roller, the measured glass transition temperature (T_g), the onset melt temperature (T_{om}) and the crystallisation temperature range (T_c) at a set laser power of 3000 W and a set deposition speed of 400 mm/s for 57 x 8 mm (substrate) laser beam. Note: the temperature beyond the "visible" nip point during deposition of ply 10 was not recorded because of an issue with the logging equipment.

3.2 Microscopy of laminated strips

The results of the microscopy analysis of the polished cross sections extracted from the unidirectional strips are reported in Figure 9 (void content) and Figure 10 (degree of intimate contact). A representative cross section for each of the three manufacturing setups is reported in Figure 11.

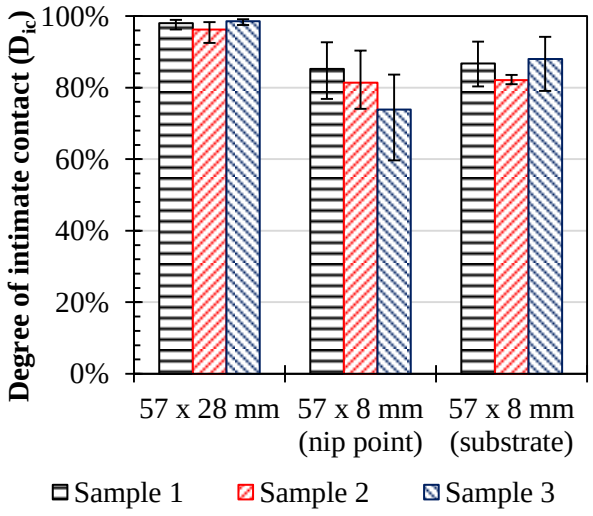

Figure 9: Measured void content. The error bars indicate the maximum and minimum.

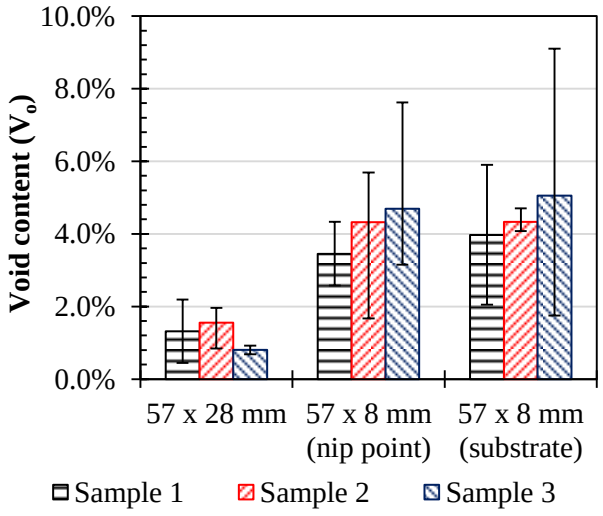

Figure 10: Measured degree of intimate contact. The error bars indicate the maximum and minimum.

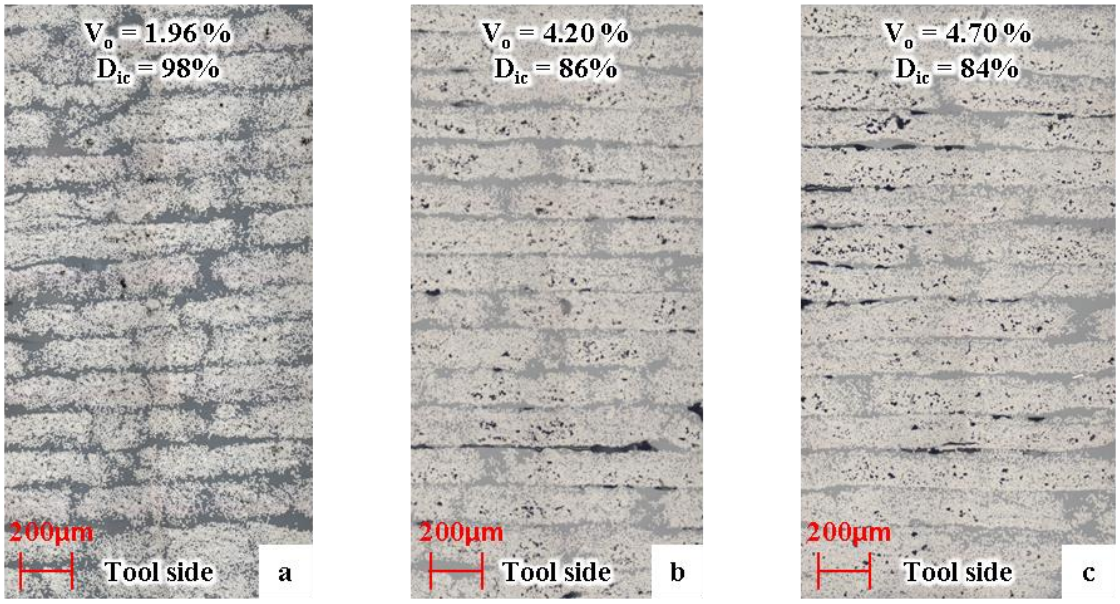

Figure 11: Typical cross section for (a) the57 x28 mm, (b) the 57 x8 mm (nip point) and (c) the 57 x 8 mm (substrate) laser beam cross section cases.

3.3 Quasi-isotropic panels

An image of each of the two quasi isotropic panels, including a representative close-up view of the surface, and results of the through transmission ultrasonic inspection, plotted as a C-scan, are reported in Figure 12 to Figure 15. The figures show the considerable difference in surface roughness and consolidation of the panels manufactured using the laser beam homogenisers delivering different laser beam cross-sectional area.

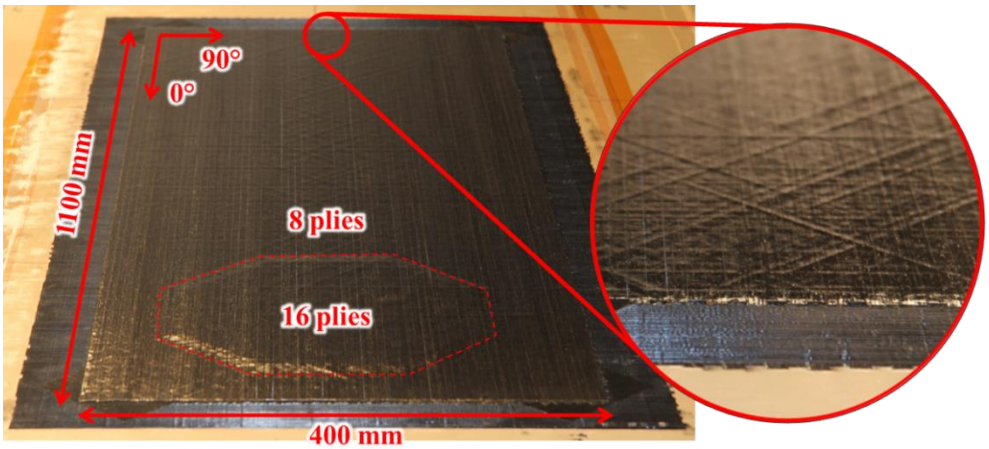

Figure 12: Panel manufactured using the 57 x 28 mm laser beam setup. Overall outlook and close-up view showing the quality of the laminate and of the material feed in particular.

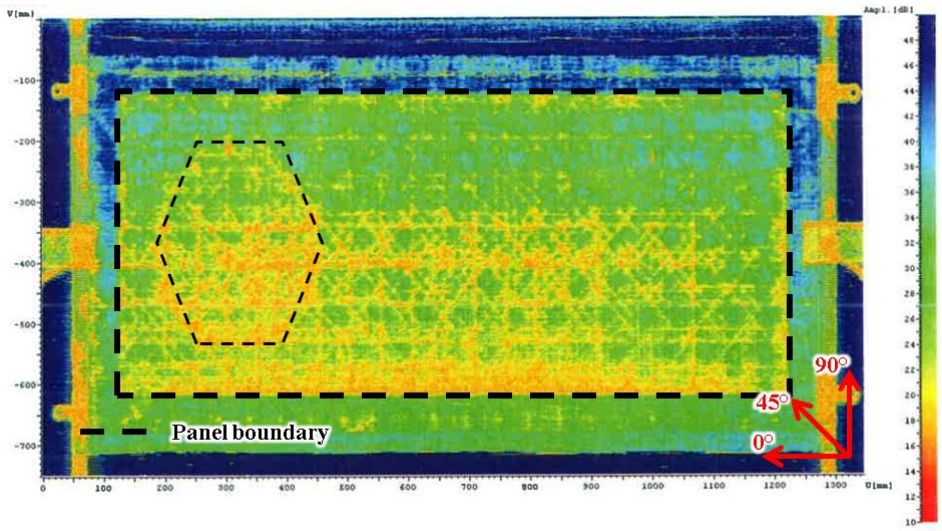

Figure 13: Through transmission ultrasonic C-scan attenuation plot of the panel manufactured using the 57 x 28 mm laser beam setup.

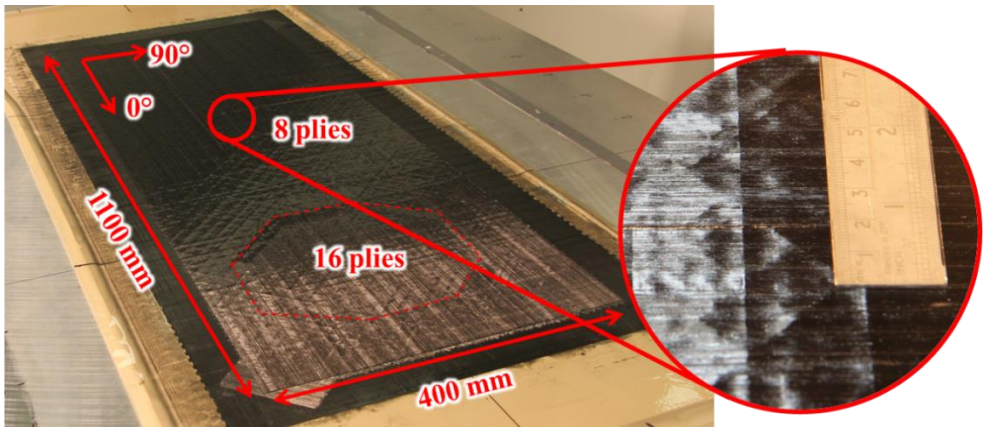

Figure 14: Panel manufactured using the 57 x 8 mm (substrate) laser beam setup. Overall panel outlook and close view showing the surface roughness of the preform.

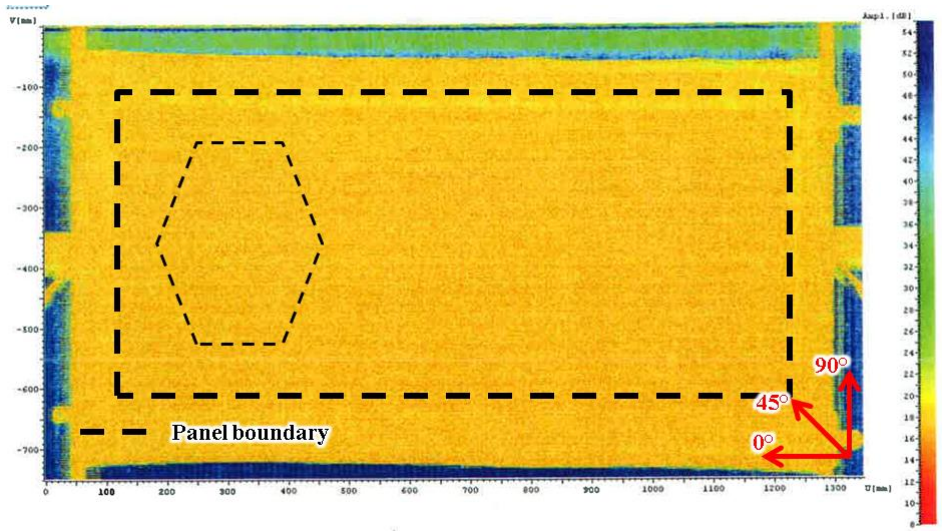

Figure 15: Through transmission ultrasonic C-scan – attenuation plot of the panel manufactured using the 57 x 8 mm (substrate) laser beam setup.

4 DISCUSSION

As seen in section 3.1 the developed numerical model is in good agreement with the thermal history observed during laser heating of the substrate for the trialled laser optics. For all cases deviation of numerical predictions for temperature history between T_{om} and T_g from measured values is below experimental uncertainty despite the observed differences between measured and predicted nip-point temperature.

The close agreement of predicted and measured through thickness temperature profile within the substrate allows differences in the process temperature-history due to varying laser-beam cross section and beam target to be efficiently assessed. In each of the simulated cases shown in Figure 6 to Figure 8, discrepancies between simulated and measured through thickness temperature profile are consistent with the model underestimating through thickness thermal diffusivity. This limitation would account for the increased nip point temperature, over-estimation of first interface temperature and suppressed peak temperature at the second interface (t = 1.0 s in Figure 6 -Figure 8). Predicted thermal diffusivity is heavily influenced by the thermal properties of the composite and the meso-structure of the laminate [7, 8]. So, based on the reported variation of thermal diffusivity for CF/PEEK prepregs in the literature [5-9], it is likely that the thermal properties of the material used in the present study is not well described by the input data taken from the literature [7]. In addition, the presented data suggests the idealised development of degree of intimate contact and linearised thermal contact resistance between plies may not adequately describe thermal diffusion in the laser assisted AFP process.

Despite challenges in predicting the observed nip-point temperature, the presented simulation approach is well suited to predicting the influence of laser optics on thermal history between onset of melt and the glass transition temperature of deposited material in constant speed AFP processes. This work forms a sound basis from which to predict evolution of inter-ply contact and material crystallinity in CF/PEEK materials deposited via laser-assisted AFP.

The experimental data presented in section 3 allows testing the following two null hypotheses:

1. At a constant deposition speed of 400 mm/s, changing the laser beam cross section from (A) 57 x 28 mm to (B) 57 x 8 mm (substrate), while regulating the power (4500 W and 3000 W respectively) to achieve the same visible nip-point temperature (389.5 ± 2.5 °C), causes no change to the laminate's meso-structure; void content (V_o) and degree of intimate contact (D_{ic}).

2. At a constant deposition speed of 400 mm/s, changing the laser power split between the substrate and the incoming tape from (A) 70 %/30 % (nip point) to (B) 100 %/0 % (substrate), while maintaining the same laser beam cross section (57 x 8 mm) and laser power (3000 W), causes no change to the laminate's meso-structure (void content and degree of intimate contact).

The nonparametric Mann-Whitney test was used to determine whether the population medians of each pair of two groups (A and B) differ [10]. With a confidence interval greater than 95%, hypothesis 1 has to be rejected for both the void content and the degree of intimate contact ($p < 0.05$) and hypothesis 2 cannot be rejected for both the parameters ($p > 0.05$) (Table 3). Changing the laser beam cross sectional area while maintaining the nip-point temperature constant changed the meso-structure measurably (hypothesis 1). On the other hand, changing the

laser power distribution while keeping the power constant caused no measurable change to the meso-structure (hypothesis 2).

Table 3: Mann-Whitney test, results.

		Median		95 % Confidence Interval (C.I.) difference between the medians (Median-A – Median-B)	p-value
		A	B		
Hypothesis 1	$\mathbf{V_o}$	0.92 %	4.21 %	- 3.94 %, - 0.99 %	0.003
	$\mathbf{D_{ic}}$	98.3 %	83.5 %	5.9 %, 17.4 %	0.001
Hypothesis 2	$\mathbf{V_o}$	4.20 %	4.21 %	- 2.38 %, 1.98 %	1.000
	$\mathbf{D_{ic}}$	79.8 %	83.5 %	-14.0 %, 3.2 %	0.158

The differences observed for the unidirectional strips are also apparent in the case of the quasi-isotropic laminates. Reducing the size of the laser cross section, while regulating the power to achieve the same nip-point temperature, causes the plies to adhere less. Limited transmission of the ultrasonic signal through the thickness of the laminate was observed in the case of the 57 x 8 mm (substrate) laser beam cross section (Figure 15), suggesting a continuous delamination. On the other hand, the preform manufactured using the 57 x 28 mm laser beam cross section shows better transmission of the ultrasonic signal through the thickness (Figure 13), and a smoother surface than for the other manufacturing setup (Figure 12 and Figure 14 respectively). It is interesting to note that in the 57 x 28 mm setup case, an area of poor consolidation is observed in the "feed" region (bottom and right hand side of the panel in Figure 12). This suggests that better laser power control at the beginning of a course is required to achieve constant consolidation across the entire panel. Nevertheless, in both cases there are no loose tapes and the plies are sufficiently adhered to make the preform easy to handle. While consolidation of the preforms will be part of future work, based on the result presented by Zhang et al [11, 12], it can be speculated that the quality of both preforms is sufficient to produce a good quality laminate through press or autoclave consolidation and that the less consolidated preform could produce a better laminate if consolidated out of autoclave in an oven.

The differences observed between the three different manufacturing setups can be related to the different thermal profiles which the three manufacturing configurations delivered. The void content and the degree of contact between the plies are expected to decrease and increase over time when the material is above its glass transition temperature and under a positive compaction pressure [13, 14]. At constant (within experimental error) nip-point temperature, reducing the laser beam cross sectional area by 3.5 times, causes a 97 % reduction of the area under the temperature versus time curve, above the glass transition temperature and under the positive compaction pressure. On the other hand, changing the position of the laser heated zone for the same laser beam cross section and power causes a comparatively insignificant 3 % change.

As the maximum temperature in the process is capped upward by the matrix degradation temperature (450-500 °C depending on the time of exposure [15, 16]). Using a laser homogeniser optics delivering a larger beam allows introducing more energy into the process while not exceeding the matrix degradation temperature. Trials showed that if the same power used for the 57 x 28 mm laser beam cross section manufacturing setup, 4500 W, was used for the 57 x 8 mm one, an unacceptable maximum temperature in excess of 500 °C would occur. A large heated zone, with correspondingly longer heating times, appears to be required to achieve high levels of compaction, adhesion between the plies and crystallinity. This is congruent with the

simulation and experimental results reported by [6], suggesting that a larger heated zone should be used at higher deposition speeds to achieve the same quality achieved at lower layup rates by maintaining the time under the laser constant for different deposition speeds.

This work shows that changing the size of the laser beam cross section by selecting different laser homogeniser optics can deliver significant changes to the preform meso-structure: the void content and the degree of intimate contact between the plies. This gives the manufacturing engineer involved in specifying the manufacturing process for a new component an additional degree of freedom which can be used to achieve the required laminate/preform meso-structure.

5 CONCLUSIONS

The work presented in this paper demonstrates the manufacturability of flat carbon fibre PEEK preforms featuring a pad-up using a laser-assisted Automated Fibre Placement machine at high rate (up to 800 mm/s). It was shown that the cross sectional area of the laser beam has a significant impact on the meso-structure (void content and degree of intimate contact) of a unidirectional strip and that the same is true for quasi-isotropic panels. On the other hand, altering the laser beam target (i.e. the distribution of the delivered power between the substrate and the incoming tapes) had a statistically insignificant impact on the meso-structure of the laminated unidirectional strips. The observed differences were traced back to the different thermal histories which the different manufacturing setups deliver to the material and, in particular, to the area under the temperature versus time curve above the matrix glass transition temperature and under positive compaction pressure. The measured differences in the laminates meso-structure are congruent with the different thermal histories in accordance with widely accepted material state models describing the compaction and expansion of voids and the evolution of the contact between the plies.

The presented numerical simulation predicts changes in laminate temperature-history caused by variation in laser beam cross section and beam target to support assessment of alternate AFP heating strategies. Development of robust material property data, prediction of resultant material state and assessing the influence of component geometry on incident radiant power in AFP processing, are promising topics for future progress in process simulation for automated fibre placement.

6 ACKNOWLEDGEMENTS

This work was supported by the National Composites Centre Core Research and Technology Programmes (www.nccuk.com). Mattia Di Francesco would like to acknowledge the support of the Engineering and Physical Sciences Research Council through the EPSRC Centre for Doctoral Training in Composites Manufacture [EP/K50323X/1].

7 REFERENCES

[1] Mondo JA, Wijskamp S, Lenferink R. Overview of thermoplastic composite ATL and AFP Technologies. In: Borgmann H, editor. International Conference and Exhibition on Thermoplastic Composites (ITHEC). Bremen, Germany: WFB Wirtschaftsförderung Bremen GmbH 2012.

[2] August Z, Ostrander G, Michasiow J, Hauber DE. Recent developments in Automated Fiber Placement of thermoplastic composites. SAMPE Journal. 2014;58(2):30-7.

[3] Collart C, Cornu YG, Ravise F. Thermoplastic materials interest to answer the industrial needs (AIRBUS Nantes). 2nd International Conference and Exhibition on Thermoplastic Composites. Bremen, Germany2014.

[4] Di Francesco M, Veldenz L, Koutsomitopoulou A, Dell'Anno G, Potter K. On the development of multi-material automated fibre placement technology. International Conference on Manufacturing Advanced Composites (ICMAC). Bristol, UK2015.

[5] Maurer D. Laser-powered thermoplastic tape placement process - simulation and optimization,. SAMPE Europe - SETEC. Tampere, Finland2014.

[6] Stokes-Griffin C, Compston P. The effect of processing temperature and placement rate on the short beam strength of carbon fibre–PEEK manufactured using a laser tape placement process. Composites Part A: Applied Science and Manufacturing. 2015;78:274-83.

[7] Stokes-Griffin CM, Compston P, Matuszyk TI, Cardew-Hall MJ. Thermal modelling of the laser-assisted thermoplastic tape placement process. Journal of Thermoplastic Composite Materials. 2013:1-18.

[8] Barasinski A, Leygue A, Soccard E, Poitou A. An improvement in thermal modelling of automated tape placement process. International conference on advances in materials and processing technologies (AMPT2010): AIP Publishing; 2011. p. 185-90.

[9] Grouve WJB. Weld strength of laser-assisted tape-placed thermoplastic composites 2012.

[10] Bass I. Six sigma statistics with Excel and Minitab. New York, NY: McGraw-Hill; 2007.

[11] Zhang D, Heider D, Advani SG, Gillespie JW. Out of Autoclave Consolidation of Voids in Continuous Fiber Reinforced Thermoplastic Composites. SAMPE; 2013.

[12] Zhang D, Heider D, Gillespie Jr JW. Volatile Removal During Out of Autoclave Processing of High Performance Thermoplastic Composites. 2014.

[13] Ranganathan S, Advani SG, Lamontia MA. A Non-Isothermal Process Model for Consolidation and Void Reduction during In-Situ Tow Placement of Thermoplastic Composites. Journal of Composite Materials. 1995;29(8):1040-62.

[14] Lee W, Springer GS. A model of the manufacturing process of thermoplastic matrix composites. Journal of Composite Materials. 1987;21:1017-55.

[15] Nicodeau C, Cinquin J, Regnier G, Verdu J. In-situ consolidation process optimisation for thermoplastic matrix composites. SAMPE 2006 Technical Conference2006.

[16] Khan MA, Mitschang P, Schledjewski R. Parametric study on processing parameters and resulting part quality through thermoplastic tape placement process. Journal of Composite Materials. 2012;47(4):485-99.